4120–4132 *Nucleic Acids Research, 2010, Vol. 38, No. 12* *Published online 1 March 2010*
doi:10.1093/nar/gkq122

Structural basis for the methylation of G1405 in 16S rRNA by aminoglycoside resistance methyltransferase Sgm from an antibiotic producer: a diversity of active sites in m^7G methyltransferases

Nilofer Husain[1], Karolina L. Tkaczuk[2,3], Shenoy Rajesh Tulsidas[1], Katarzyna H. Kaminska[2], Sonja Čubrilo[4], Gordana Maravić-Vlahoviček[4], Janusz M. Bujnicki[2,5] and J. Sivaraman[1,*]

[1]Department of Biological Sciences, 14 Science drive 4, National University of Singapore, Singapore 117543, [2]Laboratory of Bioinformatics and Protein Engineering, International Institute of Molecular and Cell Biology, Trojdena 4, 02-109 Warsaw, [3]Institute of Technical Biochemistry, Faculty of Biotechnology and Food Sciences, Technical University of Lodz, B.Stefanowskiego 4/10, 90-924 Lodz, Poland, [4]Department of Biochemistry and Molecular Biology, Faculty of Pharmacy and Biochemistry, University of Zagreb, Ante Kovačića 1, 10000 Zagreb, Croatia and [5]Laboratory of Bioinformatics, Institute of Biotechnology and Molecular Biology, Faculty of Biology, Adam Mickiewicz University, Umultowska 89, 61-614 Poznan, Poland

Received October 22, 2009; Revised February 9, 2010; Accepted February 10, 2010

ABSTRACT

Sgm (Sisomicin-gentamicin methyltransferase) from antibiotic-producing bacterium *Micromonospora zionensis* is an enzyme that confers resistance to aminoglycosides like gentamicin and sisomicin by specifically methylating G1405 in bacterial 16S rRNA. Sgm belongs to the aminoglycoside resistance methyltransferase (Arm) family of enzymes that have been recently found to spread by horizontal gene transfer among disease-causing bacteria. Structural characterization of Arm enzymes is the key to understand their mechanism of action and to develop inhibitors that would block their activity. Here we report the structure of Sgm in complex with cofactors S-adenosylmethionine (AdoMet) and S-adenosylhomocysteine (AdoHcy) at 2.0 and 2.1 Å resolution, respectively, and results of mutagenesis and rRNA footprinting, and protein-substrate docking. We propose the mechanism of methylation of G1405 by Sgm and compare it with other m^7G methyltransferases, revealing a surprising diversity of active sites and binding modes for the same basic reaction of RNA modification. This analysis can serve as a stepping stone towards developing drugs that would specifically block the activity of Arm methyltransferases and thereby re-sensitize pathogenic bacteria to aminoglycoside antibiotics.

INTRODUCTION

A substantial number of potent and widely used antibiotics inhibit the bacterial cell growth by interfering with the essential cellular process of translation (1). From early cross-linking and chemical footprinting experiments it has been learned that antibiotics bind to functionally important parts of the ribosome, such as the peptidyl transferase center, the peptide exit tunnel and the GTPase segment in the 50S subunit, or to the decoding and tRNA-binding sites in the 30S subunit. With the advances in ribosome crystallography many of the atomic aspects have been revealed that offer a detailed view of different snapshots in protein synthesis, as well as of the interaction of ribosomal antibiotics with the ribosome. We now know that the ribosomal RNA is responsible both for the enzymatic properties of the ribosome and for most of the contacts with the antibiotics (2).

Many antibiotic-producing bacteria protect themselves from the toxic effects of antibiotics by employing enzymes

*To whom correspondence should be addressed. J. Sivaraman. Tel: +65 6516 1163; Fax: +65 6779 2489; Email: dbsjayar@nus.edu.sg
Correspondence may also be addressed to Gordana Maravić-Vlahoviček. Tel: +385 1 639 4448; Fax: +385 1 639 4400; Email: gordana@pharma.hr
Correspondence may also be addressed to Janusz M. Bujnicki. Tel: +48 22 597 0750; Fax: +48 22 597 0715; Email: iamb@genesilico.pl

that add a methyl group to specific ribonucleotides in antibiotic-binding sites of the ribosome, thereby disrupting the antibiotic binding without much interference with other functions of the ribosome (2). Sgm (Sisomicin-gentamicin methylase) is a methyltransferase found in *Micromonospora zionensis* that produces the antibiotic G-52 (6-*N*-methyl-sisomicin) (3). Sgm methylates G1405 in 16S rRNA to m^7G, thereby rendering the ribosome resistant to 4, 6-disubstituted deoxystreptamine aminoglycosides, which include gentamicins and kanamycins (4,5).

Sgm belongs to the Arm (aminoglycoside resistance MTase) family, whose members share the same substrate specificity (5). Genes encoding members of this protein family have been isolated not only in antibiotic producers but also found to spread among human pathogens cultured from nosocomial infections and animal isolates, including *Pseudomonas aeruginosa* (6), *Klebsiella pneumoniae* (7) and *Escherichia coli* (7,8).

The objective of this study is to examine the relationship between Arm enzymes found in bacteria that produce antibiotics and those that emerged in resistant pathogens, as well as to make comparisons between active sites of different enzymes that introduce the m^7G modification in RNA. Thus far, we have made theoretical predictions of the Sgm structure and identified amino-acid residues responsible for catalysis of the methylation reaction (9). As a continuation of our efforts to understand the relationship between the structure and modes of action of antibiotic related MTases, we have solved the crystal structure of Sgm in complex with its cofactors AdoMet and AdoHcy at 2.0 and 2.1 Å resolutions respectively. We have also carried out structure-guided mutagenesis, isothermal titration calorimetry and protein–RNA footprinting to develop a model of Sgm–rRNA interactions and explain its mechanism of m^7G1405 methylation in 16S rRNA. These findings can be extended to other members of Arm family and facilitate the synthesis of inhibitors to incapacitate the resistance of the pathogens.

MATERIALS AND METHODS

Mutagenesis, expression and purification

Cloning of the *sgm* gene into pET-25b (+) vector with the addition of N-terminal non-cleavable $(His)_6$ tag, as well as alanine mutagenesis of residues D156, D182 and R108 were carried out as described previously (9). The constructs were co-transformed along with pGroESL into the strain BL21 (DE3) of *E. coli* for protein expression. The *E. coli* cells were cultured in 1 l LB medium at 37°C until the A_{600} nm reached 0.5–0.6. The culture was induced with 150 μM IPTG and continued to grow at 20°C overnight. Cells were harvested by centrifugation ($9000 \times g$, 30 min, 4°C), and the pellet was resuspended in the 40 ml of lysis buffer [50 mM HEPES sodium pH 8.0, 250 mM NaCl, 10% glycerol, 0.5% Triton X 100, 10 mM β-mercaptoethanol (BME), 1 protease inhibitor tablet (Roche) and 10 μl of benzonase nuclease (Novagen)].

After sonication the cell lysate was centrifuged at 17 000 rpm for 30 min at 4°C (JA-25.50 fixed angle rotor, Beckman Coulter centrifuge). The supernatant was allowed to bind to the talon beads (charged with cobalt) for an hour at 4°C and was subsequently washed twice with wash buffer (50 mM HEPES sodium pH 8.0, 250 mM NaCl, 10% glycerol, 10 mM BME and 5 mM imidazole pH 8.0). Finally the protein was eluted in two steps using the Buffer A (50 mM HEPES sodium pH 8.0, 250 mM NaCl, 10% glycerol, 10 mM BME, 100 mM imidazole pH 8.0) and Buffer B (50 mM HEPES sodium pH 8.0, 250 mM NaCl, 10% glycerol, 10 mM BME and 200 mM imidazole pH 8.0). The eluted protein was loaded onto a size exclusion column (Superdex 200, GE Healthcare) equilibrated with the buffer containing 50 mM HEPES sodium pH 8.0, 250 mM NaCl, 10% glycerol, 10 mM BME and 10 mM $MgCl_2$. The eluted Sgm was concentrated up to 9 mg/ml. Since we did not obtain structure solution using molecular replacement method we proceeded with the SelMet protein to perform the Multi-wavelength Anomalous Dispersion (MAD) experiment. A similar protocol was adopted to purify the selenomethionine (SelMet) labeled Sgm using the LeMaster medium (10).

Isothermal titration calorimetry (ITC)

For ITC experiments the Sgm in a buffer consisting of 50 mM HEPES sodium pH 8.0, 250 mM NaCl, 10% glycerol, 10 mM BME and 10 mM $MgCl_2$ was titrated against S-adenosylmethionine (AdoMet/AdoHcy, MP Biomedicals) solution prepared by dissolving the appropriate amount of AdoMet in the same buffer as the protein. The ITC experiments were carried out using VP-ITC calorimeter (Microcal, LLC) at 20°C using 0.02–0.07 mM protein in the sample cell and 2–5 mM AdoMet/AdoHcy in the injector. All samples were thoroughly degassed and centrifuged. Injection volumes of 8–10 μl per injection were used for different experiments and for each experiment; the heat of dilution for the ligand was measured. To restore the baseline, successive injections were separated by at least 4 min. The ITC data was analyzed by a single site fitting model using Origin 7.0 (OriginLab Corp.) software.

Crystallization and data collection

Purified Sgm (0.3 mM) was complexed with 5 mM of the cofactors S-adenosylmethionine (AdoMet) / S-adenosylhomocysteine (AdoHcy) [1:17 (Sgm: AdoMet/AdoHcy)]. Crystallization trials were carried out at room temperature by hanging-drop vapor-diffusion method using crystallization screens from Hampton Research (Aliso Viejo, CA, USA) and Jena Bioscience screens (Jena, Germany). Initially crystals of Sgm–cofactor complexes were obtained from the Index Screen (Hampton Screen) (11). Subsequently these conditions were optimized to obtain the diffraction quality crystals. The best crystals were obtained by mixing 1 μl of Sgm–cofactor complex with 1 μl crystallization solution (0.2 M ammonium acetate, 0.1 M Tris, pH 8.5, 25% w/v PEG 3350, 0.1 M phenol for Sgm–AdoHcy complex; 30%

PEG 5000 MME, 0.1 M sodium MES, pH 6.5, 0.2 M ammonium sulphate for Sgm–AdoMet complex) and were grown up to 5 days.

Prior to data collection, crystals were briefly soaked in a cryoprotectant consisting of the reservoir solution supplemented with 25% glycerol and flash cooled in a N_2 cold stream (100 K). A complete MAD data set was collected for both Sgm–cofactor complexes at the beamline X8C, NSLS, Brookhaven National Laboratory using a Quantum4-CCD detector (Area Detector Systems Corp Poway, CA, USA) to 2.1 and 2.0 Å resolutions for Sgm–AdoHcy and Sgm–AdoMet complexes respectively. All the datasets were processed and scaled using the program HKL2000 (12). The crystallographic statistics are provided in Table 1.

Structure solution and refinement

All the four expected selenium sites in the asymmetric unit of both Sgm complexes were located by the program SOLVE (13). The initial phases were further developed by RESOLVE (14), and the overall figure of merit was improved to 0.65 for both Sgm complexes, which made it possible to build automatically over 90% of the molecule. The remaining parts of the model were built manually using the program COOT (15). Alternating cycles of model building and refinement using the program CNS (16) with appropriate entries were made in the dictionaries for AdoMet and AdoHcy. The final model for Sgm–AdoHcy refined to 2.1 Å resolution with an R-factor of 0.20 (Rfree = 0.26), while the model for Sgm–AdoMet refined to 2.0 Å resolution with an R-factor of 0.23 (Rfree = 0.28). The PROCHECK (17) analysis of both Sgm complexes does not show any residue in the disallowed regions of Ramachandran plot (Table 1). However, it shows one residue (Thr128) in the generously allowed regions. This residue is well defined in the electron density map and it is not in the vicinity of the active-site region.

Isolation of 30S ribosomal subunits

Escherichia coli BL21 (DE3) cells were grown at 37°C in LB medium to an early log phase at an OD_{450} of 0.4–0.5. Bacteria were collected by centrifugation at low speed ($3500 \times g$) and resuspended in low magnesium buffer TM1N (50 mM Tris–HCl pH 7.5, 1 mM $MgCl_2$, 100 mM NH_4Cl). The suspension was lysed by sonication and cell debris was removed by two centrifugation cycles at $20000 \times g$ for 10 min. The lysate was loaded onto a 5–30% sucrose gradient in TM1N buffer followed by centrifugation at 18 000 rpm for 18 h in a Beckman SW-28.1 rotor. Gradient fractions were collected and the absorbance of the fractions was measured at 260 nm. 30S subunit containing fractions were pooled and dialyzed three times in 1 l of TM1N buffer for 2-h periods. The subunits were pelleted by centrifugation at 40 000 rpm

Table 1. Crystallographic data and refinement statistics

Data set	AdoMet		AdoHcy		
	Peak	Inflection	Peak	Inflection	Remote
Cell parameters (Å,°)	$a = 36.45$, $b = 68.36$, $c = 52.15$, $\beta = 93.21$	$a = 36.53$, $b = 68.41$, $c = 52.22$, $\beta = 93.23$	$a = 36.09$, $b = 68.89$, $c = 52.20$, $\beta = 93.47$	$a = 36.10$, $b = 68.92$, $c = 52.20$, $\beta = 93.4$	$a = 36.11$, $b = 68.94$, $c = 52.23$, $\beta = 93.45$
Space group	$P2_1$	$P2_1$	$P2_1$	$P2_1$	$P2_1$
Data collection					
Resolution range (Å)	50–2.0	50–1.8	50–2.1	50–2.2	50–2.2
Wavelength (Å)	0.9790	0.9798	0.9785	0.9798	0.9600
Observed reflections $>1\sigma$	108 159	158 872	113 081	98 437	98 745
Unique reflections	32 440	23 067	29 340	25 555	25 575
Completeness (%)	97.1	98.3	99.9	100	100
Overall ($I/\sigma I$)	13.9	12.9	11.4	10.5	9.9
R_{sym}[a] (%)	0.08	0.15	0.07	0.09	0.09
Refinement and quality[b]					
R_{work}[c] (no. of reflections)	0.23 (28102)		0.20 (24835)		
R_{free}[d] (no. of reflections)	0.28 (2403)		0.26 (1679)		
RMSD bond lengths (Å)	0.006		0.006		
RMSD bond angles(°)	1.4		1.4		
Average B-factors[e] (Å^2)					
Main chain	28.65		21.36		
Side chain	30.91		23.61		
Ramachandran plot					
Most favored regions (%)	90.7		90.7		
Additional allowed regions (%)	8.8		8.8		
Generously allowed regions (%)	0.4		0.4		
Disallowed regions (%)	0.0		0.0		

[a]$R_{sym} = \Sigma|I_i - \langle I \rangle|/|I_i|$ where I_i is the intensity of the ith measurement, and $\langle I \rangle$ is the mean intensity for that reflection.
[b]Reflections with $I > \sigma$ was used in the refinement.
[c]$R_{work} = |F_{obs} - F_{calc}|/|F_{obs}|$ where F_{calc} and F_{obs} are the calculated and observed structure factor amplitudes, respectively.
[d]R_{free} = as for R_{work}, but for 5% of the total reflections chosen at random and omitted from refinement.
[e]Individual B-factor refinements were calculated.

for 24 h in a Beckman 70.1 Ti rotor and resuspended in TM1N buffer.

Chemical probing of 30S subunit–Sgm complex

An amount of 10 pmol 30S ribosomal subunits were incubated with a 2-fold molar excess of Sgm methyltransferase and 1 mM AdoHcy in either modification buffer A (50 mM HEPES–KOH, pH 8.0, 10 mM $MgCl_2$, 100 mM KCl, 5 mM DTT) or B (200 mM HEPES–KOH, pH 7.8, 10 mM $MgCl_2$, 100 mM KCl) for 30 min at 37°C in 50 µl reaction mixtures. Control reactions contained no AdoHcy. The complexes were modified with either 50 µl of CMCT (18) [1-cyclohexyl-3-(2-morpholinoethyl)carbodiimide metho-*p*-toluene sulfonate; 42 mg/ml in modification buffer A] for 10 min at 37°C, or 1 µl of DEPC (19) (diethyl pyrocarbonate) for 1 h at room temperature. RNA was purified immediately with RNeasy mini kit (Qiagen), RNA cleanup protocol. The chemical modifications were monitored by primer extension analysis using AMV reverse transcriptase (Finnzymes) and 5′-Cy5 modified deoxyoligonucleotides complementary to the 16S rRNA sequences 1459–1479, 939–955 and 817–833 [(20), as modification of the protocol described in (21)]. The cDNA products of primer extension reactions were separated on 9% polyacrylamide sequencing gel and visualised on Storm imager (GE Healthcare).

Molecular docking

Macromolecular rigid-body docking of the Sgm crystal structure to the *E. coli* 30S ribosome subunit (PDB IDs: 2AVY and 2I2P) (22), and to a 33-nt long fragment comprising the target nucleoside G1405 (residues 1401–1434 of 16S rRNA) was carried out using GRAMM v1.03 (23). Additional docking was carried out for a fragment of helix 44 comprising nt 1401–1420 and 1480–1501, and its variant, in which the target nucleoside was 'flipped out' (i.e. rotated by 180 degrees). For all docking targets, the low-resolution docking mode was used to generate 1000 alternative orientations (poses) that optimized the steric complementarity between the ligand (Sgm) and the receptor (ribosome or its fragment). The following parameters were used: energy scores for repulsion and attraction were 7 and –1, respectively, grid size 64 Å, grid step 6.8 Å. The ligand was rotated with 10°-angle intervals. Poses from each round of docking were subsequently ranked according to the proximity between the residues implicated in RNA binding to the G1405 nucleoside, using the FILTREST3D server available at http://filtrest3d.genesilico.pl (Michal J. Gajda and J.M.B., manuscript in preparation). 100 top-scoring models were clustered using MAXCLUSTER (http://www.sbg.bio.ic.ac.uk/zmaxcluster/index.html), and the central pose from the largest cluster was selected as the representative model. The model of Sgm bound to the 30S subunit in a mode that enables a contact with the target base (i.e. with Sgm bound to the 3′ minor domain) was obtained by manual modification of the 30S structure with SwissPDBViewer (24).

Docking of the target guanosine to the Sgm crystal structure was carried out with SURFLEX 1.31 (25). In order to take into account the interactions of the enzyme with the RNA backbone around the target, the 3′ phosphate group was added to G1405, thus forming a guanosine 3′,5′-bismonophosphate. The structure of that ligand was prepared for docking with VegaZZ 2.2.0.54 (26). Several docking rounds with different parameters were performed. Each docking round started from 10 random orientations and conformations of the guanosine bisphosphate. Additionally, 10 docking rounds with a predefined area of docking were performed. We rejected all docking solutions, in which the methyl group acceptor, i.e. the N^7 atom of guanosine, was >3 Å from the methyl group of AdoMet. The remaining poses of the ligand were ranked according to the crash and affinity scores that describe clashes of the ligand with the receptor molecule as well as interactions within the ligand molecule, and best-scoring poses were regarded as the most likely models.

RESULTS

Overall structure

The structures of recombinant Sgm in complex with AdoMet and AdoHcy were solved by MAD method (10) from synchrotron data using SelMet labeled protein (Table 1, Figure 1). Figure 2 shows the final 2*Fo-Fc* electron density map for Sgm–AdoMet and Sgm–AdoHcy complexes. The first seven residues, His-tag at the N-terminal, and residues from Ser232 to Lys238

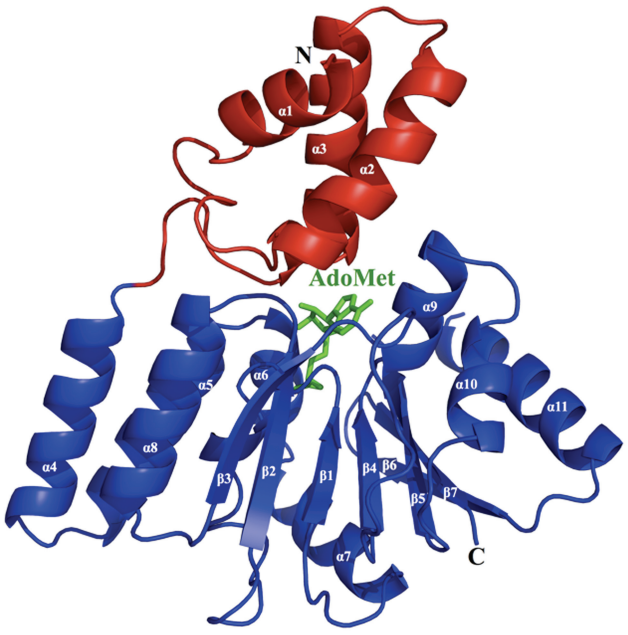

Figure 1. Structure of Sgm. Ribbon diagram of the Sgm–cofactor complex monomer. The N and C termini are labeled. The NTD and CTD domains of Sgm are colored in red and blue respectively with the core secondary structures labeled. The cofactor AdoMet is depicted in green. This figure and the following figures of this manuscript are prepared by PyMol (44).

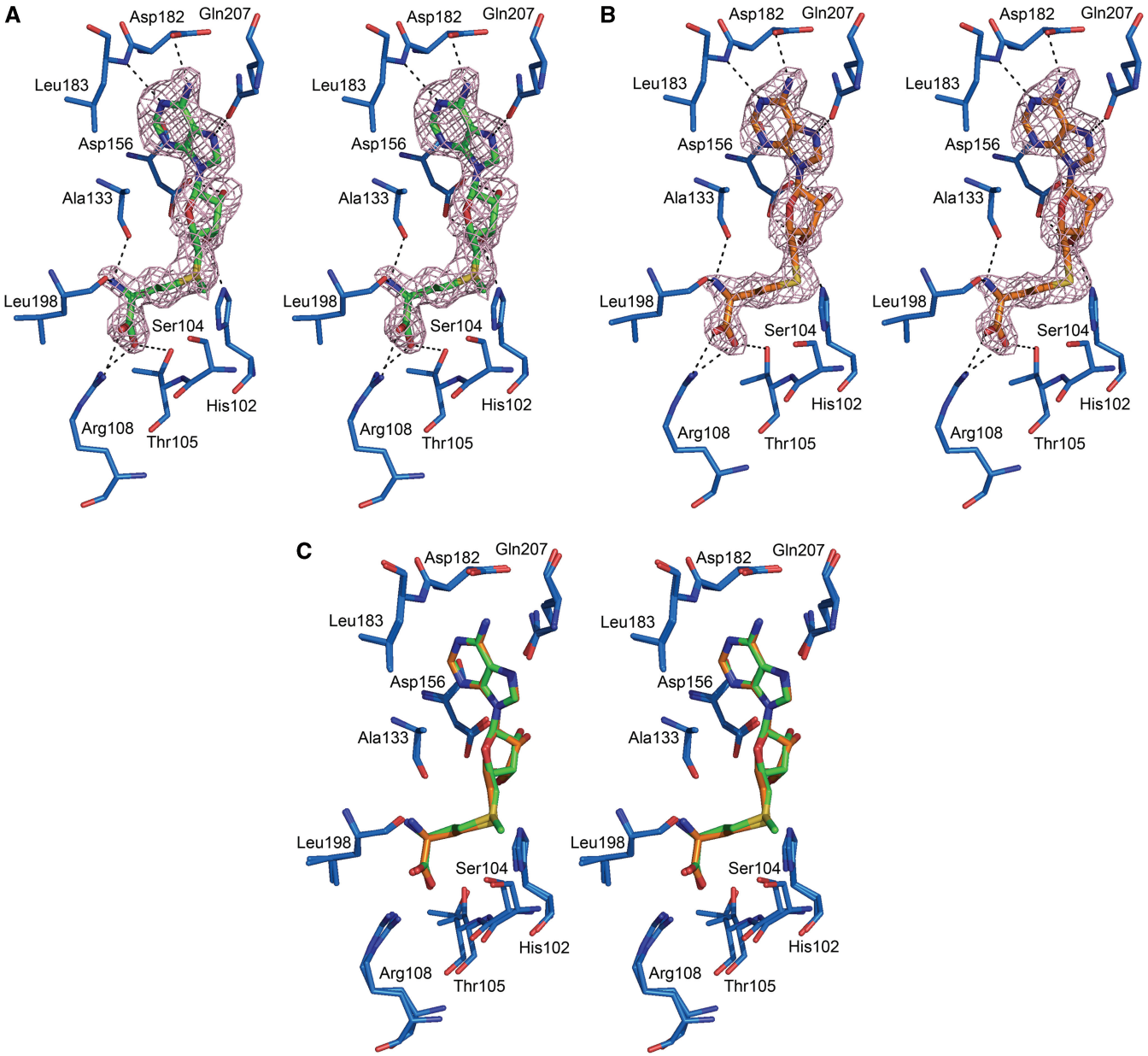

Figure 2. Stereo view of the final *2Fo-Fc* electron density maps in the active-site region of Sgm. (**A**) Sgm–AdoMet complex. (**B**) Sgm–AdoHcy complex. These maps are contoured at a level of 1σ. (**C**) Stereo view of the superposition of Sgm–AdoMet and Sgm–AdoHcy complexes. AdoHcy is shown in orange and AdoMet in green respectively.

were not well defined in the electron density map and were not modeled. The asymmetric unit consists of a Sgm complex molecule. This monomer observation is consistent with the gel filtration and dynamic light scattering (DLS) experiments (data not shown).

As predicted earlier (9), Sgm is a two-domain protein, comprising an N-terminal domain (NTD, Asp8–Pro70) and a C-terminal domain (CTD, Asn71- Gln273). The CTD adopts a typical Class I Rossmann-fold consisting of a central seven stranded β sheet (β3↑-β2↑-β1↑-β4↑-β5↑-β7↓-β6↑) surrounded by three α helices on each side (27). At the N-terminus, this core of the CTD is extended by two additional α-helices that are not conserved in the RFM superfamily. The NTD is a bundle of three α-helices with a left-handed twist, exhibiting the RuvA CTD-like fold (Supplementary Figure 1A). The active site is located in the CTD, which interacts with the cofactors AdoMet and AdoHcy. The superposition of these two complexes reveals a root mean square deviation (RMSD) of 0.2 Å for 259 Cα atoms. Both structures are nearly identical with negligible differences in the active-site region (Figure 2C). The crystal structure reveals that the previously published theoretical model (9) was accurate for the homology-modeled RFM core (residues 111–267; RMSD = 2.32 Å), however it has incorrectly predicted the structure of the de novo-modeled N-terminal extension.

Table 2. Structural matches of the Sgm protein, according to DALI (43): 10 most closely related protein structures, followed by three (very remotely related) structures of other known m^7G MTases acting on different RNA substrates

DALI match	PDB id	*Z*-score	RMSD [Å]	eq. residues	seq.id. [%]	Organism	Protein
1	3frh	**27.6**	**1.9**	237	**32**	*Escherichia coli*	RmtB
2	3fri	**27.3**	**2.0**	237	**32**	*Escherichia coli*	RmtB
3	3b89	**27.2**	**2.0**	237	**32**	*Escherichia coli*	RmtB
4	3fzg	**20.2**	**2.5**	188	**31**	*Escherichia coli*	ArmA
5	2ex4	13.1	3.0	174	10	*Homo sapiens*	Adrenal gland protein AD-003
6	1xtp	12.5	3.1	177	10	*Leishmania major*	Hypothetical protein LMAJ004091AAA
7	3jwh	12.5	2.9	156	15	*Anabaena variabilis*	Small RNA MTase HEN1
8	3jwj	12.5	3.0	158	15	*Anabaena variabilis*	Small RNA MTase HEN1
9	3jwi	12.4	3.0	157	13	*Clostridium thermocellum*	Small RNA MTase HEN1
10	1ve3	12.3	3.1	168	13	*Pyrococcus horikoshii*	Hypothetical protein PH0226
(...)							
165	1ri2	10.6	3.1	156	13	*Encephalitozooon cuniculi*	mRNA cap 0 MTase Ecm1
304	1jsx	9.7	3.4	150	11	*Escherichia coli*	23S rRNA m^7G1835 MTase RsmG
454	2fca	8.1	3.4	132	8	*Bacillus subtilis*	tRNA m^7G46 MTase TrmB

Only the best superimposed protein chain per individual structure has been included. Strongest structural and sequence similarities to the Arm family members are shown in bold.

A search for structurally similar proteins within the PDB performed with DALI (Table 2) revealed, as expected, highest similarity to MTases from the Arm family: RmtB (solved independently by Schmitt *et al.* (28), PDB codes 3frh and 3fri and by the New York Structural GenomiX Research Consortium (NYSGXRC), PDB code 3b89, DOI 10.2210/pdb3b89/pdb) and ArmA [(28) PDB code 3fzg]. It is important to emphasize that these homologous MTases belong to a small branch of the Arm family (proteins from pathogens), while the structure of Sgm presented herein is the first representative of the large subfamily (proteins from antibiotic producers) (5,9). Sequences of Sgm and RmtB (as well as Sgm and ArmA) exhibit 31% sequence identity and their structures exhibit high structural similarity (Supplementary Figure S1B). Subsequent matches in the PDB are other RFM-fold proteins with predicted or determined methyltransferase activity: human adrenal gland protein AD-003, and small RNA MTase HEN1. The similarity between Sgm and all proteins except ArmA and RmtB is limited to the RFM core of the CTD, and does not include the additional two α-helices or the NTD. Interestingly, other known structures of m^7G MTases from the same RFM superfamily exhibited relatively low DALI scores, indicating considerable structural divergence.

DALI search for the isolated NTD structure revealed similarity to ArmA methyltransferase (DALI Z-score 8.0, RMSD = 1.9 Å for 57 Cα atoms), but also to proteins with the RuvA CTD-like fold, e.g. RuvA from *Mycobacterium tuberculosis* (PDB code 2h5x; DALI Z-score 7.0, RMSD = 1.5 Å for 48 Cα atoms), and NAD dependent malic enzyme (PDB code 1gz3; DALI Z-score 5.5, RMSD = 2.8 Å for 57 Cα atoms). NTD also shows weak structural similarity to Ub-pathway associated (UBA) and Ub-like (UBL) domains of Ubiquitin-receptor proteins of the proteasome (PDB code 2oob; DALI Z-score 4.9, RMSD = 2.0 Å for 42 Cα atoms). This domain is often involved in substrate recognition, and is often found in proteins that bind nucleic acids (e.g. RuvA or the elongation factor TFIIS). The NTD of Sgm is highly basic (calculated pI = 10.46) compared with the CTD which is acidic (calculated pI = 5.57). Thus, it is tempting to speculate that the NTD of Sgm is likely to dictate the substrate specificity through the interactions with rRNA, to select the specific region of 16S rRNA to be methylated.

Sgm–AdoMet/AdoHcy interactions

Residues such as His102, Ser104, Thr105, Arg108, Ala133, Asp156, Asp182, Leu183, Leu198 and Gln207 line up the cofactor-binding site of Sgm (Figure 2). These residues are found to interact with the AdoMet and AdoHcy, and are likely to play a key role in the methylation of G1405. There are 11 hydrogen-bonding contacts (<3.2 Å) between Sgm and AdoMet/AdoHcy. Leu183, Gln207 and the conserved Asp182 interact with the adenosine moiety of the cofactors, whereas the conserved Asp156 coordinates the 2′ and 3′ hydroxyls of the ribose. Other conserved residues such as Leu198, Ala133 and Arg108 interact with the carboxypropyl moiety of AdoMet/AdoHcy.

Sequence conservation in Sgm and its homologs

Sequence analyses of Sgm revealed that it belongs to the Arm family of MTases, which groups together 32 homologs [as of September 2009, a significant expansion from 19 members in our earlier study (9)]. Their hosts are mainly antibiotic producers Streptomyces and Micromonospora species, as well as pathogens. The overall sequence identities between Sgm and its homologs is over 30%. Supplementary Figure S2 shows the multiple sequence alignment of all Arm sequences detectable in databases. The CTD of Sgm has the nine conserved motifs characteristic for the RFM superfamily of MTases (29). In enzymes from this superfamily, residues from motifs X, and I to IV typically interact with the AdoMet molecule, and residues from motifs IV, VI and VIII and sometimes X are usually involved in

binding of the substrate. Motifs V and VII are typically poorly conserved and include residues important for the stability of the RFM fold. The structures of Sgm–AdoHcy and Sgm–AdoMet complexes presented here reveal the exact role of individual residues. Interestingly, in our searches we identified new, strongly diverged members of the Arm family from *N. equitans* (NEQ545, the first archaeal ortholog) and *C. thermocellum* (Cthe3180). While they exhibit perfect conservation of motifs in the C-terminal catalytic domain, their NTDs appear to be strongly diverged in sequence. Computational structure predictions (secondary structure prediction as well as protein fold-recognition, see Matrials and methods section) suggest that these diverged N-terminal regions also exhibit propensity to fold into helical structures similar to those observed in Sgm, ArmA and RmtB MTases. However, the NEQ545 sequence lacks one helix and the Cthe3180 sequence appears to possess one additional helix. It is unclear if these two proteins exhibit the same function as orthodox members of the Arm family, nonetheless they should be classified as Arm members in the evolutionary sense. Phylogenetic analysis (Supplementary Figure S3) confirms that NEQ545 and Cthe3180 are the most diverged members of the Arm family and shows that they have originated from the group of MTases from pathogens, rather than those from antibiotic producers.

ITC analyses

Interactions between Sgm with both cofactors were studied by isothermal titration calorimetry (ITC) (Figure 3, Supplementary Figure S4). The dissociation constant (K_d) for AdoMet was determined to be 18 μM with $N = 0.90$, which is consistent with the results obtained by Savic *et al.* (30) for Sgm and AdoMet. The dissociation constant (K_d) for AdoHcy, which was not reported before, is 300 μM with N = 1.0. We have performed the ITC experiments on the mutants D156A, D182A and R108A with both AdoMet and AdoHcy using the same conditions as the native Sgm with cofactors. A complete loss of binding was observed when the Sgm mutants D156A, D182A or R108A were titrated against both AdoMet and AdoHcy (Figure 3, Supplementary Figure S4). Interaction between Sgm and guanine nucleotide was also studied by ITC. Guanosine 5′-monophosphate was used because guanosine did not solubilize in the buffer used. The dissociation constant (K_d) was determined to be 1.4 mM with $N = 1.1$. The low affinity suggests that Sgm requires contacts with the RNA flanking the guanosine moiety.

RNA footprinting analysis of Sgm interactions with the 30S subunit

Sgm has been found to act on fully assembled 30S ribosomal subunit (SSU) (4). Chemical footprinting with CMCT and DEPC was carried out on *E. coli* 30S subunits to determine the sites of Sgm–ribosome interaction. After incubation with Sgm and chemical modification with CMCT (specific for nucleotides G and U) and DEPC (specific for nucleotide A) we screened with primer extension from different parts of 16S rRNA that are spatially close to G1405, the target of Sgm methylation (Supplementary Figure S5, Figure 4). Despite our efforts to analyze entire helix 44 (nt 1404–1497) with a primer used previously by Kaberdina *et al.* (31), in our hands this primer could not be properly extended. Using primer 1459–1479 we were therefore able to detect changes only in one strand of helix 44, starting with U1450, down to C1302 in helix 42. We have also used primers 939–955 and 817–833. Nucleotides found to be protected in the presence of Sgm included A694, A695, A718, G734, G733, U751, G755, U757, G765, A790, U793, U798, G887, G895, G1387, G1401, G1405 (the methylatable target), U1414, G1423, G1426, G1435, U1445 and U1450. At the same time nt G774, G775, G776, G1323, U1341, U1358, U1376, C1393, A1394, C1407, A1408, C1412, A1413, U1436, U1440 and U1444 were found to be deprotected in the presence of Sgm. This suggests that a conformational changes occur in the SSU upon its interactions with Sgm that allow the enzyme to access the target nucleotide G1405, which is otherwise buried in the crystal structure of 30S subunit.

Modeling of Sgm-substrate complex

To gain insight into the possible mechanism of Sgm–target-base interactions, we used a high-resolution-docking method SurFlex in order to position G1405 (in the form of a 3′5′-bismonophosphate) into the active site of the Sgm–AdoMet complex (see 'Materials and Methods' section). The ligand was treated as a flexible molecule, while the receptor (Sgm–AdoMet complex) was kept rigid. The best pose [score: affinity 6.03, crash –1.25 (self –0.37)] was found to fit very well into the Sgm active site, without any large conformational changes of the protein (Figure 5). According to the docking model, the methyl group of K199 from motif IV may interact with the O^6 atom of the base. This residue potentially assisted by the hydroxyl group of S104, and most likely positions guanosine in appropriate orientation with respect to the methyl group donor. F64 from the NTD and P229 from motif VI form the walls of the guanosine-binding pocket and are likely to be important for the stable binding of the target base in the active site. Other possible interactions include hydrogen-bonding between E107 with the N^2 and possibly also N^1 atoms of the target base (if the side chain of E107 undergoes appropriate reorientation). The hydroxyl groups of T206 and Y244 may coordinate either of the phosphate groups.

In order to predict the mode of protein-substrate interactions, we attempted to dock the Sgm–AdoMet complex to the 30S subunit structure, with a restraint imposed as to minimize the distance between the methyl group of AdoMet and the target nucleoside G1405 (see 'Materials and methods' section for details). In all docking solutions, the protein could reach only the solvent-exposed face of the helix, and no models could be obtained with the target base closer than 15 Å to the methyl group of AdoMet. This macromolecular docking analysis indicates that Sgm cannot access G1405 while the 30S subunit is in the crystal-like conformation and, in agreement with our

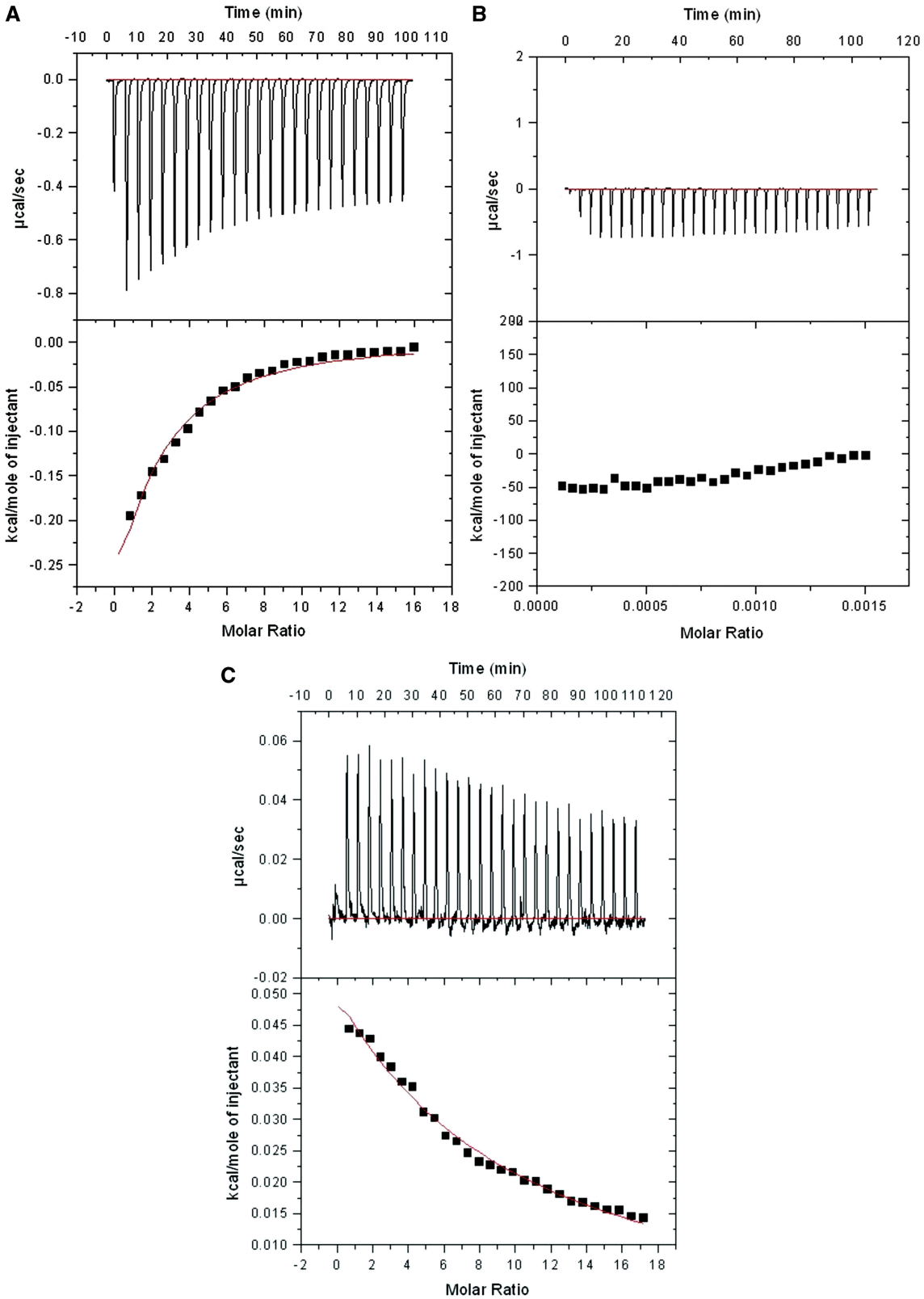

Figure 3. ITC analyses. (**A**) Sgm–AdoHcy titration. (**B**) Sgm mutant R108A-AdoMet titration. (**C**) Sgm–GMP titration. The upper panels show the injection profile after baseline correction and the bottom panels show the integration (heat release) for each injection (except the first one).

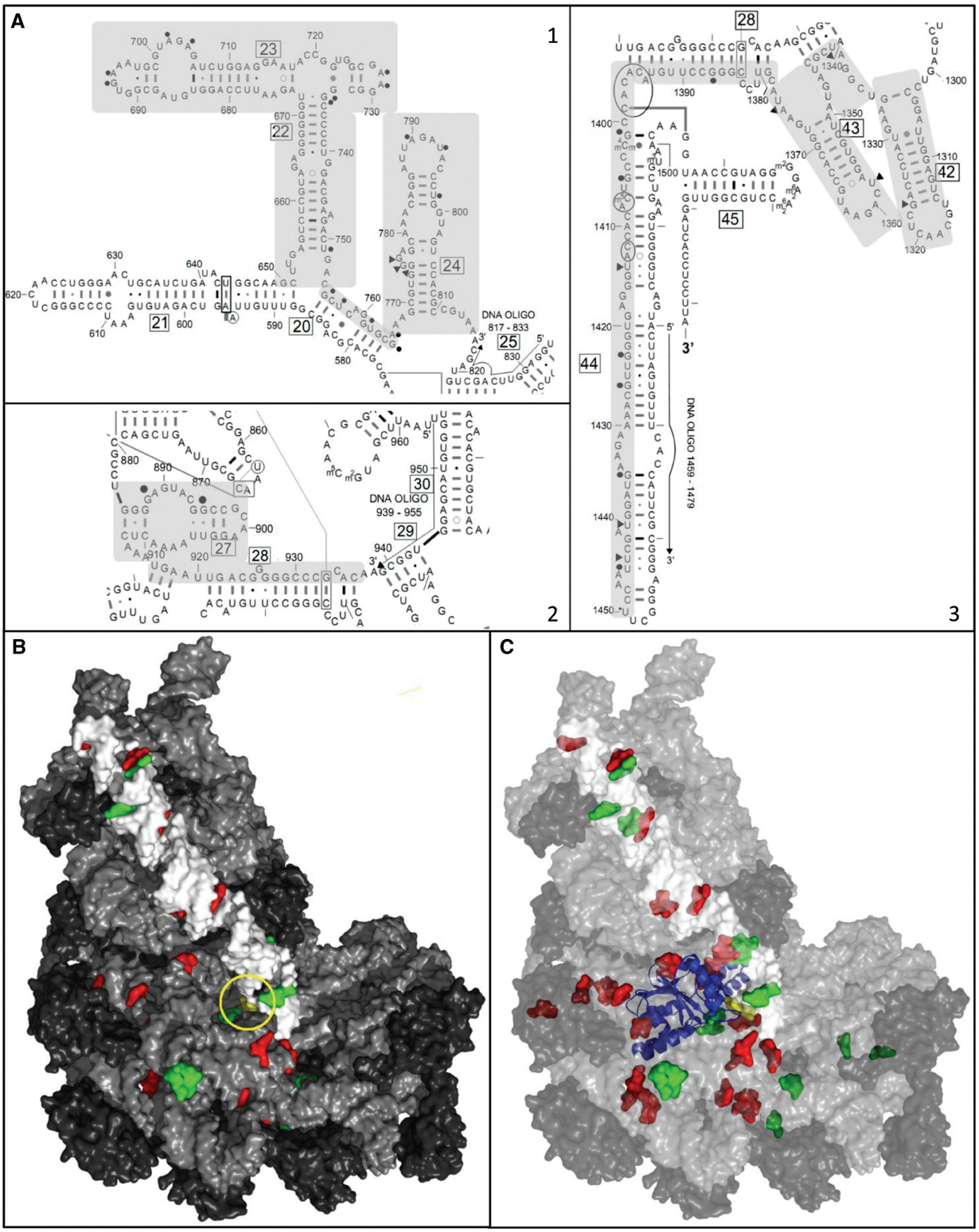

Figure 4. Schematic presentation of the Sgm–30S ribosomal subunit complex. (**A**) Summary of the footprinting results. Sections of the 16S rRNA that were analyzed by primer extension are shaded in grey. Nucleotides protected upon Sgm binding are indicated with a black dot, whereas exposed nucleotides are indicated with a black triangle symbol. For circle indicated regions, structural change was observed upon Sgm binding to 30S subunits. Helix numbering is presented in boxes. After chemical footprint, rRNA was extended with reverse transcriptase with primers complementary to regions: (1) 817–833, (2) 939–955 and (3) 1459–1479. (**B**) Mapping of footprinting data onto the 30S structure. Components of the 30S subunit are shown in the surface representation, ribosomal proteins are indicated in dark gray, 16S rRNA is indicated in light gray with the exception of helix 44 (residues 1400–1499), shown in white. Results of the footprinting experiments are color coded as follows: residues relatively more reactive in the footprinting experiment are shown in green, residues less reactive in the footprinting experiment are shown in red. The target G1405 is shown in yellow and is additionally indicated by a yellow circle. (**C**) Extreme steric clashes between Sgm and the 30S subunit occur, if the enzyme is docked to its target in helix 44 without any conformational changes. The 30S structure is color-coded as in panel B, but semi-transparent. Sgm is shown as a solid ribbon in blue; target G1405 is shown in yellow and helix 44 is shown in white.

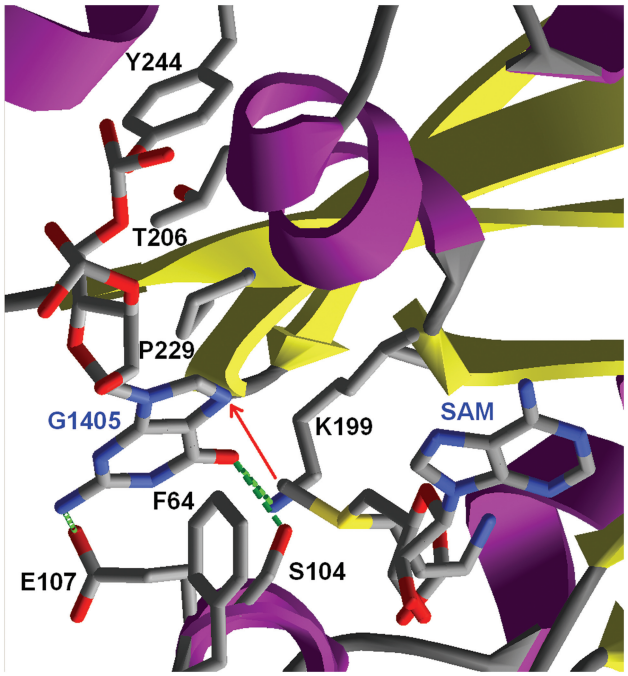

Figure 5. Model of guanosine 3′5′-bismonophosphate docked to the Sgm–AdoMet complex. Residues 1–63 have been omitted for clarity. The protein backbone is shown as a ribbon (with helices in violet and strands in yellow). Residues predicted to interact with the target nucleoside are shown as sticks and labeled; contacts predicted in detail are shown as green broken lines. A contact between the transferrable methyl group and the target N^7 atom (distance = 3 Å) is shown by a red arrow.

RNA footprinting results, suggests that a conformational rearrangement must occur to expose G1405 and enable methylation. Interestingly, docking of Sgm to helix 44 detached from the rest of the 30S subunit has led to a model with the protein active site close to the target nucleoside G1405. In this position, the target base could be positioned within the active site of Sgm by simply rotating it out of the helix (Supplementary Figure 6). Base flipping has been documented for both DNA- and RNA-modifying enzymes and is believed to be the dominant mechanism used by these enzymes to access target bases that are normally non-accessible due to secondary and/or tertiary interactions in the nucleic-acid molecule (32). The orientation of the base flipped out of docked helix 44 is essentially identical to that obtained by docking of 3′5′-bismonophosphate. This suggests that both docking simulations produced the geometrically most reasonable solution for the problem of protein–target interactions.

DISCUSSION

Conservation of sequence, structure and function in the Arm family

Sgm belongs to the Arm family, whose members methylate the N^7 atom of G1405 in bacterial 16S rRNA, thereby conferring resistance to aminoglycoside antibiotics. Previous analyses established that Arm MTases are composed of two domains, with the large C-terminal RFM-fold domain responsible for cofactor binding and catalysis, and the small NTD most likely involved in RNA binding (9,28). According to phylogenetic analyses, the Arm family can be subdivided into two subfamilies, a large one represented by presumably ancestral MTases from antibiotic producers (e.g. Sgm and KgmB), and a smaller one with MTases that have been acquired by pathogenic bacteria via horizontal gene transfer (e.g. ArmA and RmtB) (5,9). Thus far, crystal structures have been determined only for ArmA and RmtB, members of the small subfamily (28). We have determined the first structure of an Arm enzyme from an antibiotic producer, a representative of the large subfamily, which provides evidence for a common architecture and close evolutionary relationship between both types of MTases.

The Sgm complex structures with AdoMet and AdoHcy highlighted the importance of the residues R108, G135 (in motif I), D156 (in motif II) and D182 (in motif III) as crucial for the interaction of Sgm with the cofactors. D156 and D182 were previously shown to be indispensable for rendering bacteria resistant to kanamycin and gentamicin (9,30) and their role in AdoMet binding was confirmed by ITC (30). Residues homologous to D156 and D182 are functionally conserved in Rossmann-fold MTases and form hydrogen bonds with the cofactors. As anticipated, mutation of D156A, D182A or R108A disrupted the binding, as determined by the ITC titrations. It is worth mentioning here that these three residues alone provide at least five H-bonding contacts with AdoMet/AdoHcy. Therefore, we conclude that these three residues play a crucial role in the catalytic activity of the Sgm and the mutation of any one of them abolishes the binding of the cofactors. Structural similarity between Arm MTases from pathogens and antibiotic producers and evolutionary conservation of residues predicted to be involved in substrate binding strongly suggest that the mode of enzyme–substrate interactions is conserved in both types of MTases.

Our analysis also provides the first characterization of interactions between an Arm family MTase and its substrate, the 30S subunit. We have analyzed the RNA–Sgm contacts in detail by chemical probing following by primer extensions. Figure 4B shows the results of RNA footprinting mapped onto the crystal structure of the 30S subunit. The target nucleoside G1405 is base-paired with C1496 at the base of long helix 44 formed by the 3′ minor domain of 16S rRNA, buried in the structure, and its N^7 atom is not accessible for methylation, hence a conformational change must occur in order for the methylation to take place (Figure 4C). This is supported both by observations that short CA stretches upstream and downstream of G1405 show increased reactivity in the presence of Sgm. Interestingly, changes in propensity of 16S rRNA residues to react with hydroxyl radicals upon interaction with Sgm are not localized exclusively to the region surrounding the target guanine residue, but are scattered around different parts of the 30S subunit, both in sequence and in space. Both the results of footprinting and docking analyses suggest that the

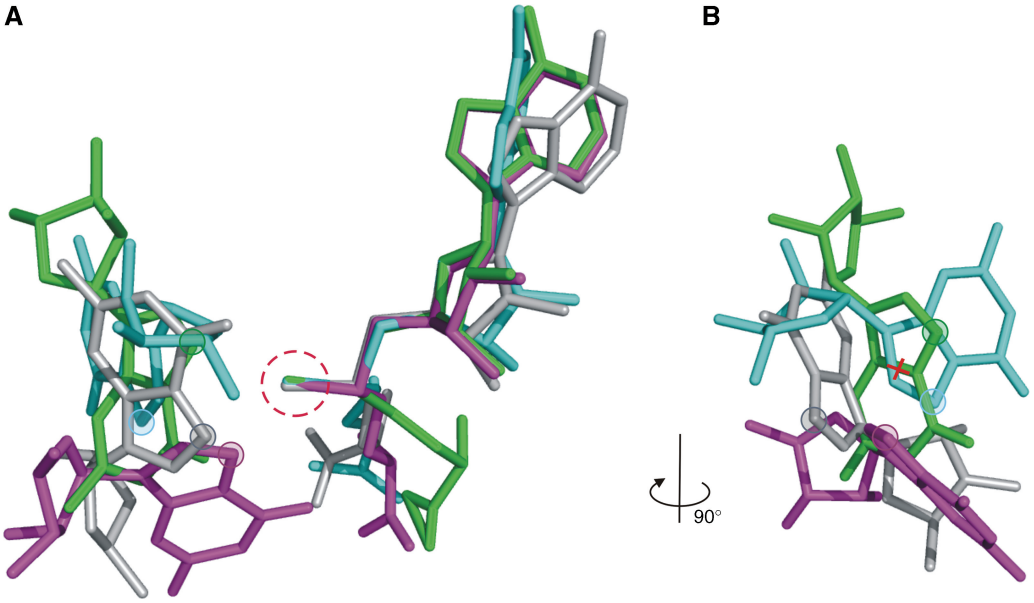

Figure 6. Orientation of AdoMet and guanosine in m^7G MTases Ecm1 (position of AdoMet and guanosine determined experimentally), Sgm (docked guanosine), TrmB (docked AdoMet and guanosine) and RsmG (docked guanosine). Both ligand and the substrate have been presented in wireframe representation. Green structures correspond to positions occupied in Sgm, cyan in TrmB, magenta in RsmG and grey in Ecm1. On the left panel (**A**) the methyl group of AdoMet is indicated by a hashed circle, while on the right panel (**B**) it is not shown explicitly, instead its position is indicated by a red cross. The target N^7 atom of guanosine in different complexes is indicated by a semi-transparent circle in the same color as the nucleoside.

conformational change of the 30S subunit upon Sgm binding involves the rearrangement of helix 44, and most likely base-flipping of G1405. However, we were unable to build a model of a 30S–Sgm complex that would satisfactorily explain all our footprinting data. Hence, conformational changes that are expected to occur in 16S rRNA upon Sgm binding are most likely complex and involve multiple rearrangements of spatially distant elements that probably have a global character.

Convergence of catalytic mechanisms among different m^7G MTases from the same RFM superfamily

Based on sequence analyses and comparison of conserved residues in active sites of m^7G MTases from various families it has been postulated that they may bind the target base in different ways (33,34). However, thus far the structure-based model of MTase–AdoMet–guanosine interactions has been available only for cap 0 MTases that modify G0 in eukaryotic mRNA (35). In addition to the Arm family of 16S rRNA:m^7G1405 MTases analyzed in this work, crystal structures are available for representatives of the tRNA:m7G46 (TrmB) MTase family (36) and 16S rRNA:m^7G527 (RsmG) MTase family [previously known as GidB (37)]. A molecular model has been also proposed for the Bud23 protein, a representative of a family of eukaryotic MTases involved in m^7G1575 modification in 18S rRNA (38). However, none of these structures have been solved with the substrate, and the details of protein-guanosine contacts and the mechanism(s) of action remain unknown.

We constructed models of protein–AdoMet complexes (by copying the coordinates of AdoMet from homologous structures) and carried out guanosine 3′5′-monobisphosphate docking for TrmB from *Bacillus subtilis* (PDB code: 2fca), and RsmG from *E. coli* (PDB code: 1jsx), as described in Materials and methods section. Figure 6 illustrates the experimentally determined orientation of both ligands in the cocrystal structures of cap 0 MTase Ecm1 from *Encephalitozoon cuniculi* [a combination of Ecm1–AdoMet and Ecm1–m^7Gppp complexes, PDB codes 1ri2 and 1ri4 (35)] and the predicted orientation of ligands in docking models constructed here for Sgm, TrmB and RsmG. We have also mapped sequence conservation in each respective protein family onto the representative structures and identified the potential key ligand-binding residues (Table 3). In the comparative sequence analysis we have also included the model of Bud32, whose accuracy is insufficient for high-resolution docking, but allows for prediction of potential catalytic residues.

The docking analysis and sequence conservation mapping reveal that both the cofactor-binding residues (in particular the three acidic residues coordinating the methionine, ribose and adenosine moieties of AdoMet) and the cofactor-binding mode are conserved among all m^7G MTases included in this study (the only exception is the lack of carboxylate residue in motif III of RsmG). On the other hand, the target guanosine-binding residues are quite different between all proteins, and likewise, the (predicted) conformation and orientation of the docked guanosine varies greatly. Although there are analogies in the type of amino acids that interact with the target guanosine (e.g. the use of Pro, Tyr, or Phe to stabilize the base), their position is typically non-homologous, and the 3D

Table 3. Key residues implicated in binding of AdoMet (high conservation) and target guanosine (high variation)

Protein	Sgm	TrmB	RsmG	Ecm1	Bud23
PDB code	3lcu, 3lcv	2fca	1jsx	1ri2, 1ri4	model
Methylation	16S rRNA	tRNA	23S rRNA	mRNA cap0	18S rRNA
Site	m^7G1405	m^7G46	m^7G1835	m^7Gppp(Np)n	m^7G1575
motif I	D131	E44	D71	D70	D53
HB to Met in AdoMet-					
motif II	D156	E69	D96	D94	D77
HB to ribose in AdoMet-					
motif III	D182	D96	R123	D122	D99
HB to adenine in AdoMet			uncertain		
motif IV	K199	P119	R139	F141, Y145	S118, Q121
G-binding	HB	Stacking	Role uncertain	Stacking, HB	HB
motif VI	P229	D154	NA	NA	Y159
G-binding	Stacking	HB			Role uncertain
motif VIII	NA	Y193	NA	Y284	K194
G-binding		Stacking or HB		HB	HB?
Other regions	F64, E107 (N-domain)	NA	R52, H53 (motif X)	V220, E225 (insertion)	Unknown
G-binding	Stacking, HB		Role uncertain	Stacking, HB	

HB, hydrogen-bonding; NA, not available. '?' indicates uncertainty of the predicted contact.

arrangements are completely different, demonstrating alternative solutions for the methylation of the N^7 atom of guanine.

Our docking models suggest that at least four different m^7G MTase families evolved independent ways of recognizing the target guanosine. This is in agreement with the results of our phylogenetic analysis of the entire RFM superfamily, in which the aforementioned families of m^7G MTases do not form a single branch on the tree and most likely have evolved independently (K.L.T. and J.M.B., unpublished data). This situation resembles the polyphyletic evolution of 2′-*O*-ribose MTases, which are known to belong to different folds, SPOUT (39) and RFM (40), and even within the RFM-fold exhibit several different architectures of the active site (41).

The finding that other m^7G MTases [especially the cap 0 MTase that is essential for the human cells (42)] exhibit different modes of protein–ligand interactions, suggests that Arm-specific inhibitors can be developed that will not interfere with other physiologically important m^7G methylations. Thus, the results of our analyses provide a stepping stone for the design of inhibitors against the medically important Arm family of MTases. In particular, the guanosine-binding site identified in the Sgm structure (and by extension, in homologous structures of ArmA and RmtB MTases) can be used as receptor for structure-based virtual screening.

SUPPLEMENTARY DATA

Supplementary Data are available at NAR Online.

ACKNOWLEDGEMENTS

We thank Dr Anand Saxena for assistance in data collection. Data for this study were measured at beam lines X12C and X29 of the National Synchrotron Light Sources, BNL. We are grateful to the GlaxoSmithKline Research Centre Zagreb Ltd. for the use of the Storm imager, especially to Kruno Nujić for the technical assistance. We thank Dr S. Sunita for her suggestions in Sgm expression and purification.

FUNDING

Biomedical Research Council of Singapore (BMRC), A*STAR research grant (R154000362305); Polish Ministry of Science grants N301 2396 33 and HISZPANIA/152/2006 (to J.M.B.); EU 6FP grant EURASNET (LSHG-CT-2005-518238) (to K.H.K.); Polish Ministry of Science Ph.D. grant (N301 105 32/3599) and 'START' fellowship from the Foundation for Polish Science (to K.L.T.); Croatian Ministry of Science (grant 006-0982913-1219), ICGEB (grant CRP/CRO08-02) and FP6 (grant #043682 'EuroPharm') (to G.M.V.); National University of Singapore (NUS) research scholarship (to N.H.). Funding for open access charge: BMRC, A*STAR grant Singapore (R154000362305).

Conflict of interest statement. None declared.

REFERENCES

1. Tenson,T. and Mankin,A. (2006) Antibiotics and the ribosome. *Mol. Microbiol.*, **59**, 1664–1677.
2. Poehlsgaard,J. and Douthwaite,S. (2005) The bacterial ribosome as a target for antibiotics. *Nat. Rev. Microbiol.*, **3**, 870–881.
3. Kojic,M., Topisirovic,L. and Vasiljevic,B. (1992) Cloning and characterization of an aminoglycoside resistance determinant from *Micromonospora zionensis*. *J. Bacteriol.*, **174**, 7868–7872.
4. Cubrilo,S., Babic,F., Douthwaite,S. and Maravic Vlahovicek,G. (2009) The aminoglycoside resistance methyltransferase Sgm impedes RsmF methylation at an adjacent rRNA nucleotide in the ribosomal A site. *RNA*, **15**, 1492–1497.
5. Savic,M., Lovric,J., Tomic,T.I., Vasiljevic,B. and Conn,G.L. (2009) Determination of the target nucleosides for members of two families of 16S rRNA methyltransferases that confer resistance to partially overlapping groups of aminoglycoside antibiotics. *Nucleic Acids Res.*, **37**, 5420–5431.

6. Yokoyama,K., Doi,Y., Yamane,K., Kurokawa,H., Shibata,N., Shibayama,K., Yagi,T., Kato,H. and Arakawa,Y. (2003) Acquisition of 16S rRNA methylase gene in *Pseudomonas aeruginosa*. *Lancet*, **362**, 1888–1893.
7. Yan,J.J., Wu,J.J., Ko,W.C., Tsai,S.H., Chuang,C.L., Wu,H.M., Lu,Y.J. and Li,J.D. (2004) Plasmid-mediated 16S rRNA methylases conferring high-level aminoglycoside resistance in *Escherichia coli* and *Klebsiella pneumoniae* isolates from two Taiwanese hospitals. *J. Antimicrob. Chemother.*, **54**, 1007–1012.
8. Gonzalez-Zorn,B., Teshager,T., Casas,M., Porrero,M.C., Moreno,M.A., Courvalin,P. and Dominguez,L. (2005) ArmA and aminoglycoside resistance in *Escherichia coli*. *Emerg. Infect. Dis.*, **11**, 954–956.
9. Maravic Vlahovicek,G., Cubrilo,S., Tkaczuk,K.L. and Bujnicki,J.M. (2008) Modeling and experimental analyses reveal a two-domain structure and amino acids important for the activity of aminoglycoside resistance methyltransferase Sgm. *Biochim. Biophys. Acta*, **1784**, 582–590.
10. Hendrickson,W.A., Horton,J.R. and LeMaster,D.M. (1990) Selenomethionyl proteins produced for analysis by multiwavelength anomalous diffraction (MAD): a vehicle for direct determination of three-dimensional structure. *EMBO J.*, **9**, 1665–1672.
11. D'Arcy,A., Mac Sweeney,A., Stihle,M. and Haber,A. (2003) The advantages of using a modified microbatch method for rapid screening of protein crystallization conditions. *Acta Crystallogr. D Biol. Crystallogr.*, **59**, 396–399.
12. Otwinowski,Z. and Minor,W. (1997) Processing of X-ray diffraction data collected in oscillation mode. *Methods Enzymol.*, **276**, 307–326.
13. Terwilliger,T.C. and Berendzen,J. (1999) Automated MAD and MIR structure solution. *Acta Crystallogr. D Biol. Crystallogr.*, **55**, 849–861.
14. Terwilliger,T.C. (2003) Automated main-chain model building by template matching and iterative fragment extension. *Acta Crystallogr. D Biol. Crystallogr.*, **59**, 38–44.
15. Emsley,P. and Cowtan,K. (2004) Coot: model-building tools for molecular graphics. *Acta Crystallogr. D Biol. Crystallogr.*, **60**, 2126–2132.
16. Brunger,A.T., Adams,P.D., Clore,G.M., DeLano,W.L., Gros,P., Grosse-Kunstleve,R.W., Jiang,J.S., Kuszewski,J., Nilges,M., Pannu,N.S. *et al.* (1998) Crystallography & NMR system: a new software suite for macromolecular structure determination. *Acta Crystallogr. D Biol. Crystallogr*, **54(Pt 5)**, 905–921.
17. Laskowski,R.A., MacArthur,M.W., Moss,D.S. and Thornton,J.M. (1993) PROCHECK: a program to check the stereochemical quality of protein structures. *J. Appl. Crystallogr.*, **26**, 283–291.
18. Kofoed,C.B. and Vester,B. (2002) Interaction of avilamycin with ribosomes and resistance caused by mutations in 23S rRNA. *Antimicrob. Agents Chemother.*, **46**, 3339–3342.
19. Ziehler,W.A. and Engelke,D.R. (2001) Probing RNA structure with chemical reagents and enzymes. *Curr. Protoc. Nucleic Acid Chem.*, Chapter 6, Unit 6 1.
20. Ying,B.W., Fourmy,D. and Yoshizawa,S. (2007) Substitution of the use of radioactivity by fluorescence for biochemical studies of RNA. *RNA*, **13**, 2042–2050.
21. Stern,S., Moazed,D. and Noller,H.F. (1988) Structural analysis of RNA using chemical and enzymatic probing monitored by primer extension. *Methods Enzymol.*, **164**, 481–489.
22. Schuwirth,B.S., Borovinskaya,M.A., Hau,C.W., Zhang,W., Vila-Sanjurjo,A., Holton,J.M. and Cate,J.H. (2005) Structures of the bacterial ribosome at 3.5 Å resolution. *Science*, **310**, 827–834.
23. Vakser,I.A. (1997) Evaluation of GRAMM low-resolution docking methodology on the hemagglutinin-antibody complex. *Proteins*, **29(Suppl 1),** 226–230.
24. Guex,N. and Peitsch,M.C. (1997) SWISS-MODEL and the Swiss-PdbViewer: an environment for comparative protein modeling. *Electrophoresis*, **18**, 2714–2723.
25. Jain,A.N. (2003) Surflex: fully automatic flexible molecular docking using a molecular similarity-based search engine. *J. Med. Chem.*, **46**, 499–511.
26. Pedretti,A., Villa,L. and Vistoli,G. (2004) VEGA–an open platform to develop chemo-bio-informatics applications, using plug-in architecture and script programming. *J. Comput. Aided Mol. Des.*, **18**, 167–173.
27. Bujnicki,J.M. (1999) Comparison of protein structures reveals monophyletic origin of the AdoMet-dependent methyltransferase family and mechanistic convergence rather than recent differentiation of N^4-cytosine and N^6-adenine DNA methylation. *In Silico Biol.*, **1**, 175–182.
28. Schmitt,E., Galimand,M., Panvert,M., Courvalin,P. and Mechulam,Y. (2009) Structural bases for 16 S rRNA methylation catalyzed by ArmA and RmtB methyltransferases. *J. Mol. Biol.*, **388**, 570–582.
29. Kozbial,P.Z. and Mushegian,A.R. (2005) Natural history of S-adenosylmethionine-binding proteins. *BMC Struct. Biol.*, **5**, 19.
30. Savic,M., Ilic-Tomic,T., Macmaster,R., Vasiljevic,B. and Conn,G.L. (2008) Critical residues for cofactor binding and catalytic activity in the aminoglycoside resistance methyltransferase Sgm. *J. Bacteriol.*, **190**, 5855–5861.
31. Kaberdina,A.C., Szaflarski,W., Nierhaus,K.H. and Moll,I. (2009) An unexpected type of ribosomes induced by kasugamycin: a look into ancestral times of protein synthesis? *Mol. Cell*, **33**, 227–236.
32. Cheng,X. and Blumenthal,R.M. (2002) Cytosines do it, thymines do it, even pseudouridines do it–base flipping by an enzyme that acts on RNA. *Structure (Camb)*, **10**, 127–129.
33. Bujnicki,J.M. and Rychlewski,L. (2001) Sequence analysis and structure prediction of aminoglycoside-resistance 16S rRNA:m^7G methyltransferases. *Acta Microbiol. Pol.*, **50**, 7–17.
34. De Bie,L.G., Roovers,M., Oudjama,Y., Wattiez,R., Tricot,C., Stalon,V., Droogmans,L. and Bujnicki,J.M. (2003) The *yggH* gene of *Escherichia coli* encodes a tRNA (m^7G46) methyltransferase. *J. Bacteriol.*, **185**, 3238–3243.
35. Fabrega,C., Hausmann,S., Shen,V., Shuman,S. and Lima,C.D. (2004) Structure and mechanism of mRNA cap (guanine-N7) methyltransferase. *Mol. Cell.*, **13**, 77–89.
36. Zegers,I., Gigot,D., van Vliet,F., Tricot,C., Aymerich,S., Bujnicki,J.M., Kosinski,J. and Droogmans,L. (2006) Crystal structure of *Bacillus subtilis* TrmB, the tRNA (m7G46) methyltransferase. *Nucleic Acids Res.*, **34**, 1925–1934.
37. Romanowski,M.J., Bonanno,J.B. and Burley,S.K. (2002) Crystal structure of the *Escherichia coli* glucose-inhibited division protein B (GidB) reveals a methyltransferase fold. *Proteins*, **47**, 563–567.
38. White,J., Li,Z., Sardana,R., Bujnicki,J.M., Marcotte,E.M. and Johnson,A.W. (2008) Bud23 methylates G1575 of 18S rRNA and is required for efficient nuclear export of pre-40S subunits. *Mol. Cell. Biol.*, **28**, 3151–3161.
39. Tkaczuk,K.L., Dunin-Horkawicz,S., Purta,E. and Bujnicki,J.M. (2007) Structural and evolutionary bioinformatics of the SPOUT superfamily of methyltransferases. *BMC Bioinformatics*, **8**, 73.
40. Feder,M., Pas,J., Wyrwicz,L.S. and Bujnicki,J.M. (2003) Molecular phylogenetics of the RrmJ/fibrillarin superfamily of ribose 2'-O-methyltransferases. *Gene*, **302**, 129–138.
41. Tkaczuk,K.L., Obarska,A. and Bujnicki,J.M. (2006) Molecular phylogenetics and comparative modeling of HEN1, a methyltransferase involved in plant microRNA biogenesis. *BMC Evol. Biol.*, **6**, 6.
42. Chu,C. and Shatkin,A.J. (2008) Apoptosis and autophagy induction in mammalian cells by small interfering RNA knockdown of mRNA capping enzymes. *Mol. Cell. Biol.*, **28**, 5829–5836.
43. Holm,L. and Sander,C. (1993) Protein structure comparison by alignment of distance matrices. *J. Mol. Biol.*, **233**, 123–138.
44. DeLano,W.L. (2002) *DeLano Scientific*. San Carlos, CA, USA.